Giant dipole effect and second-harmonic generation in quantum wires biased with a magnetic field

A. Svizhenko, A. Balandin, and S. Bandyopadhyay

Citation: Journal of Applied Physics **81**, 7927 (1997); doi: 10.1063/1.365378
View online: https://doi.org/10.1063/1.365378
View Table of Contents: http://aip.scitation.org/toc/jap/81/12
Published by the American Institute of Physics

Giant dipole effect and second-harmonic generation in quantum wires biased with a magnetic field

A. Svizhenko
Department of Electrical Engineering, University of Notre Dame, Notre Dame, Indiana 46556

A. Balandin[a] and S. Bandyopadhyay[b]
Department of Electrical Engineering, University of Nebraska, Lincoln, Nebraska 68588

(Received 7 November 1996; accepted for publication 17 March 1997)

We have theoretically studied giant dipoles associated with transitions between magneto-electric subbands in a quantum wire subjected to a transverse magnetic field. The strengths of these dipoles and their resonant frequencies can be varied with the magnetic field which then allows one to tune the emission wavelength of these transitions. The large magnitude of the dipole moments also leads to a strong second-harmonic component of the dielectric susceptibility that can be utilized for nonlinear optical applications such as second-harmonic generation, limiting, mixing, optical switching, etc. © *1997 American Institute of Physics.* [S0021-8979(97)02612-1]

I. INTRODUCTION

Direct intraband transitions between the quantized states (subbands) of the conduction band in a quantum well is a well-researched topic.[1] It has been shown both experimentally and theoretically that such transitions have very large dipole moments and narrow bandwidths. Strong infrared absorption, associated with transitions between the lowest two electronic subbands in a GaAs quantum well, was observed long ago by a number of experimental groups.[2] Recently, population inversion between the second and third subbands of a quantum well has been established unambiguously and has led to demonstration of the celebrated quantum cascade laser.[3] The energy separation between the subbands in a quantum well or wire can be varied by an external magnetic field which then allows one to realize a continuously tunable laser or light-emitting-device. Moreover, the field can induce forbidden transitions that make additional frequency ranges accessible, thus permitting flexible device design.

Another potential use of magnetic field biasing of quantum wells or wires is in nonlinear optics. Nonlinear optical properties stem from higher order dielectric susceptibilties. Specifically, the second-order susceptibility $\chi^{(2)}$ is responsible for such phenomena as mixing and second-harmonic generation. It is well known that even-order susceptibilities vanish in structures with inversion symmetry. Consequently, finite second-order susceptibilities can be obtained in such structures only if the inversion symmetry of the conduction-band potential is broken either by an external electric field or by the intentional growth of an asymmetric well. Obviously, the former is the preferred method since an electric field can be continuously varied which allows one to tune the degree of symmetry breaking and the magnitude of $\chi^{(2)}$. This method, however, has a practical shortcoming. An electric field tilts the potential barriers of the well thereby allowing carriers to escape by tunneling or thermionic emission. This is especially serious in GaAs/AlGaAs systems where the barrier height is relatively small. It has been pointed out that the electronic states in a quantum confined system biased by a transverse electric field are never true bound states since the particles can always lower their energy by escaping from the well.[4] Therefore, these states have a finite lifetime, which broadens the transitions.

To overcome this shortcoming, one can adopt magnetostatic biasing. A magnetic field can break inversion symmetry without tilting potential barriers and promoting carrier escape. A transverse magnetic field applied to a quantum wire exerts a Lorentz force on an electron moving along the wire. As a result, its wave function (in any subband) will be skewed towards one edge of the wire. This skewing does not tilt potential barriers to first order (the barriers may tilt slightly because of a second-order effect associated with space charges and the self-consistent (Hall) electric field). However, it effectively breaks inversion symmetry since it causes a net charge to accumulate at either edge of the wire (the charges at the two edges have opposite signs as in the classical Hall effect). This leads to a nonvanishing even-order susceptibility in a symmetric structure. The skewing has another subtle effect. The degree to which the wave function is skewed is *different in different subbands* since an electron has different kinetic energies and hence experiences different Lorentz forces in different subbands. As a result, transitions between subbands whose wave functions have the same parity — which are forbidden without a magnetic field — are now allowed since the parities are altered by different amounts in different subbands by the different degrees of skewing.[5]

This article is organized as follows. In Section II, we describe the theoretical formulation, followed by results. Finally, in Section IV, we present the conclusions.

II. THEORY

We consider a quantum wire as shown in Fig. 1 with a magnetic field applied along the z direction. The thickness

[a]On leave from the University of Notre Dame.
[b]Electronic mail: bandy@engrssl.unl.edu

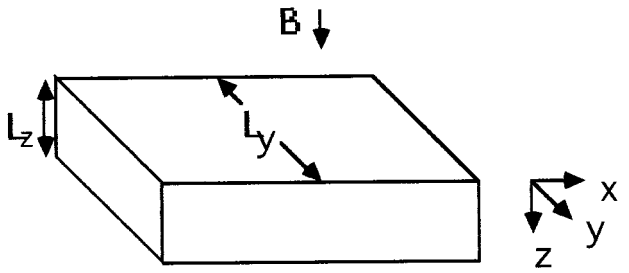

FIG. 1. An electron waveguide (quantum wire) subjected to a magnetic field along the z axis. The width of the wire is much larger than the thickness.

along the z direction is so small (and consequently the subband separation in energy is so large) that, for the range of photon energies considered, an electron cannot be excited (by real transition) into a subband which has more than two nodes along the z direction. Such a transition will not be accessible in energy. This restriction, coupled with the fact that a magnetic field does not affect the z component of the electron wave function, allows us to drop the z component from further consideration. The width of the wire along the y direction is however large enough that subbands with more than two nodes along the y direction are accessible in energy.

In the framework of the envelope function approximation (EFA), an electron wave function can be written as the product of a Bloch wave function, periodic with the atomic lattice spacing, and an envelope wave function, describing the nonperiodic behavior. Consequently, the wave function of an electron for a given wave vector k along the x direction, in the nth magnetoelectric subband, at a magnetic field B can be written as

$$\Phi_n(x,y,k,B,t)=\Psi_n(x,y,k,B)u_n(x,y,z,k)e^{-jE_n(k,B)t/\hbar}, \tag{1}$$

where $\Psi_n(x,y,k,B)$ is an envelope function, $u_n(x,y,z,k)$ is a Bloch function of a conduction band and $E_n(k,B)$ is the dispersion relation of the nth magnetoelectric subband at a flux density B. The Bloch wave functions are assumed to be s states which is the usual case for semiconductors where $\hat{J}=1/2$ for the conduction band.

The envelope function can be further decomposed into a plane wave along the unconfined x direction and a confined component along the y direction. Thus,

$$\Psi_n(x,y,k,B)=\chi_n(y,k,B)e^{jkx}. \tag{2}$$

Using the electric dipole approximation, we can write the matrix element of photoinduced intersubband transitions within the conduction band as[6]

$$d_{f,i}(k,B)=e\int \chi_f(y,k,B)\,\hat{\eta}\cdot\vec{r}\chi_i(y,k,B)d\vec{r} \times \int u_f^*(x,y,z,k)u_i(x,y,z,k)d\Omega, \tag{3}$$

where $d\Omega$ is a volume element, $\hat{\eta}$ is the unit vector along the direction of the incident photon polarization, $\vec{r}=x\vec{a}_x+y\vec{a}_y$ is the two-dimensional radius vector, and subscripts i,f stand for initial and final states respectively. The exponential term of Eq. (2) is not present in Eq. (3) since, for photoinduced transitions ($k_f=k_i$), the product of the exponential function and its complex conjugate are exactly unity. The volume overlap of the Bloch functions is also unity for s states with the same wave vector. Now, if we assume that the incident light is polarized along the y direction so that $\hat{\eta}=\hat{a}_y$, the above equation simplifies to

$$d_{f,i}(k,B)=e\langle\chi_f|y|\chi_i\rangle=e\int_{-W/2}^{W/2} y\chi_f(y,k,B)\chi_i(y,k,B)dy, \tag{4}$$

where W is the width of the quantum wire along the y direction.

One should note here that if there is no magnetic (or electric) field applied, the envelope functions χ_i are just particle-in-box states and the dipole moment in Eq. (4) is nonzero only for the transitions between subband states of opposite parity. For a symmetric square potential well, these dipole elements (between any two states n and m) are independent of the wave vector k and can be found analytically[1] by evaluating the integral in Eq. (4).

$$d_{f,i}=e\langle\chi_f|y|\chi_i\rangle=eW\frac{8}{\pi^2}\frac{mn}{(m^2-n^2)^2}, \quad \text{if } n \text{ and } m \text{ have opposite parity}$$
$$=0, \quad \text{otherwise.} \tag{5}$$

However, when a magnetic field is applied, the skewing of the wave functions changes the integral in Eq. (4) and alters the selection rules. Generally, the skewing causes three effects. First, it makes the dipole moment depend on the wave vector k (since the degree of skewing depends on k). Second, it reduces the dipole moment for transitions between states of opposite parity [since the integral in Eq. (4) decreases], and third, it allows forbidden transitions between states of the same parity [since the integral in Eq. (4) no longer vanishes for states of the same parity].

It is clear from Eq. (4) that, to calculate the dipole moments in the presence of a magnetic field, all we need to compute are the wave functions $\chi_{f,i}(y,k,B)$ at a given magnetic field B, for given magnetoelectric subbands f and i, and for a given wave vector k. This is achieved via a numerical (finite difference) solution of the Schrödinger equation following the prescription of Ref. 7. Once this is done, we can calculate the dipole moment in Eq. (4) for any chosen intersubband transition at any chosen magnetic field and for any chosen wave vector.

In the limit of high magnetic fields, when the magnetic length $l(=\sqrt{\hbar/eB})\ll W$, one can again obtain an analytical expression for the dipole moment $d_{f,i}$. In this case, the magnetostatic confinement predominates over electrostatic confinement and the envelope functions $\chi_n(y,k,B)$ can be approximated by harmonic-oscillator wave functions:

$$\chi_n(y,k,B)\equiv\chi(y-y_k,B) =N_nH_n(\alpha,y-y_k)e^{-\frac{1}{2}\alpha^2(y-y_k)^2}, \tag{6}$$

where $N_n=(\alpha/\pi^{1/2}2^2n!)^{1/2}$ is a normalization constant, $H_n(\alpha,y)$ is the nth Hermite polynomial, $y_k=\hbar k/eB$, and

$$\alpha=\sqrt{\frac{eB}{\hbar}}=\frac{1}{l}. \tag{7}$$

In order to evaluate the integral in Eq. (4) analytically, we extend the limits of integration to infinity assuming that the wave function tail is negligible at the boundaries of the wire (i.e. at $y=\pm W/2$). This is a very reasonable assumption in a high confining magnetic field. The resulting analytical expression for the dipole moment is

$$d_{f,i}(B)=e\langle\chi_f|y|\chi_i\rangle=el\left(\frac{n+1}{2}\right)^{1/2}, \quad \text{if } m=n+1 \tag{8}$$

$$=el\left(\frac{n}{2}\right)^{1/2}, \quad \text{if } m=n-1$$

$$=0, \quad \text{otherwise.}$$

The physical significance of the two analytical limits, $B\to 0$ and $B\to\infty$, is obvious. At zero field, the dipole is determined by the width of the wire $d_{f,i}\sim eW$, and at the high field limit it is determined by the magnetic length $d_{f,i}\sim el$. This is what one would expect intuitively. At zero field, the dipole is confined electrostatically with the wire width being a measure of this confinement while at high magnetic field, the dipole is confined magnetostatically and the magnetic length is the corresponding measure of this confinement.

III. RESULTS

A. Intraband dipoles

We now present results of our calculations. The physical parameters used for the numerical calculations correspond to a GaAs quantum wire with relative dielectric constant $\epsilon_r=12.9$, and effective mass $m_e=0.067m_0$ where m_0 is the free electron mass.

In Fig. 2, we show the dependence of the dipole moment $d_{f,i}(k,B)$ for three transitions ($e1$-$e2$, $e2$-$e3$, and $e1$-$e3$) on the wave vector k when a magnetic field of 1 T is applied (following usual practice, the transitions are numbered by the subband indices). The dipoles corresponding to transitions between states of opposite parity ($e1$-$e2$ and $e2$-$e3$) have maxima at $k=0$ and then decrease with increasing wave vector. This can be easily understood as follows. At zero wave vector (no translational velocity) these states do not experience any Lorentz force and hence the wave functions are not skewed. As the wave vector k increases, the translational velocity and the Lorentz force experienced increase. Consequently, the envelope wave functions are skewed more and more and the dipole moment decreases. Real transitions between states of the same parity are forbidden at zero magnetic field, but at a finite magnetic field, they are forbidden only at $k=0$ when there is no translational velocity and no Lorentz force to skew the wave functions. With increasing k, the wave functions are increasingly skewed and the dipole moment of forbidden transitions increases. In our chosen

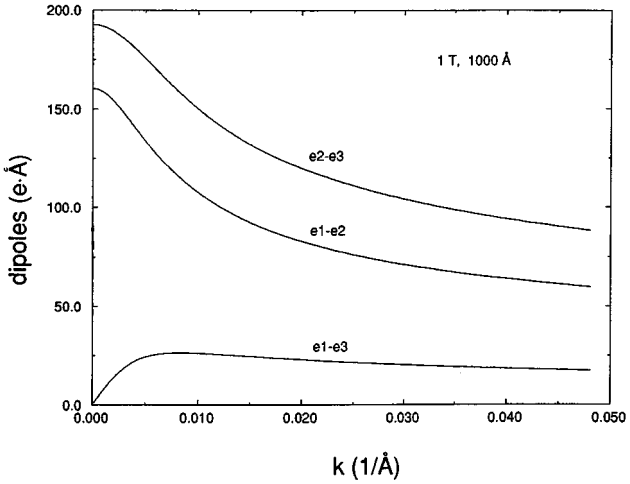

FIG. 2. Dipole moments for various intersubband transitions as functions of the propagating wave vector k for a magnetic flux density of 1 T. At zero translational velocity ($k=0$) the dipole of transition $e1$-$e3$ vanishes. The GaAs quantum wire is 1000 Å wide.

prototype wire, d_{e1-e3} reaches a maximum of 28 e-Å at $k=0.0051$ Å and then decreases gradually ultimately reaching zero. This intriguing *nonmonotonic* dependence on k is explained later on. However, at this point, it is interesting to note that a fairly large forbidden dipole moment of ~ 30 e-Å can be achieved in realistic structures at a moderate magnetic field of 1 T.

Fig. 3 presents the dipole moments for the same transitions as a function of magnetic flux density. The propagation wave vector k is chosen to be 0.01/Å. At zero magnetic field, a nonvanishing dipole matrix element occurs only for transitions between states of opposite parity ($e1$-$e2$, $e2$-$e3$) as expected from Eq. (5). This equation also allows us to estimate the strengths of these zero-field dipoles to be 180 e-Å for $e1$-$e2$ and 195 e-Å for $e2$-$e3$ transitions. As we can see from Fig. 3, these values are in excellent agreement with our

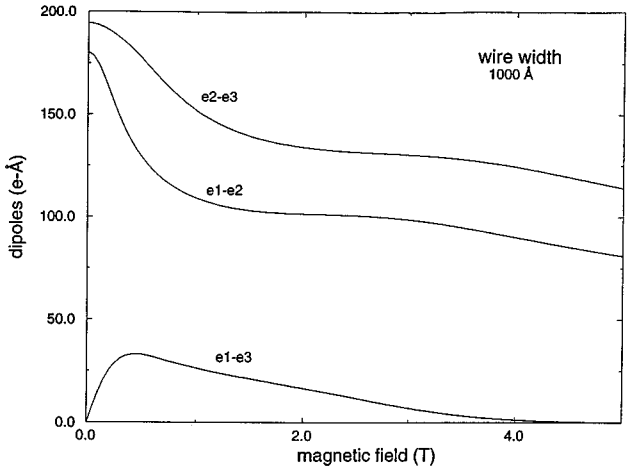

FIG. 3. The dipoles of three intersubband transitions as functions of the applied magnetic field. The dipole d_{e1-e3} peaks at a magnetic flux density of 0.3 T. The wire width is the same as that in Fig. 2.

numerical results. From the analytical expression in Eq. (8), we can estimate the strength of the $e1$-$e2$ dipole to be 66 e-Å at a magnetic flux density of 15 T. This number also agrees with our numerical result. The $e1$-$e3$ dipole vanishes at both zero field (because of the spatial symmetry of the particle-in-a-box states) and at high fields because of the symmetry of the Landau states or Hermite polynomials. This behavior is consistent with Eqs. (5) and (8). Only at intermediate fields, when the wave functions of the subbands are a hybrid between particle-in-a-box states and Hermite polynomials (and thus ''nonsymmetric'' in space), is this transition allowed. This immediately tells us that d_{e3-e1} must have a *nonmonotonic* dependence on the magnetic flux density B and indeed it does.

Let us now examine the nonmonotonic behavior of d_{e3-e1} more closely. This transition is forbidden at zero field since the wave functions of the first and third subbands have the same parity. At low magnetic fields, the parities are altered by the skewing of the wave functions and consequently d_{e3-e1} is no longer zero but increases with the magnetic field. It reaches a maximum of about 30 e-Å and then decreases. This latter decrease is related to the following effect. For a fixed wave vector k, a sufficient increase in the flux density B forces the traversing states (''skipping orbits'' or ''edge states'') to condense into closed cyclotron orbits (Landau levels) that are no longer skewed by the magnetic field to the wire edge since they have no translational velocity and hence no Lorentz force. While edge states have a skewed wave function that is not symmetric in space, cyclotron orbits have a wave function that is symmetric about the orbit center y_k. Note that y_k depends only on k and B. Therefore, at a fixed k, the wave functions of the first and third Landau levels are symmetric about a *common* center. Whenever this kind of symmetry holds, d_{e3-e1} vanishes. Therefore, the dipole moment d_{e3-e1} decreases gradually to zero at high magnetic field with the onset of Landau condensation.

The same physics can be elucidated in a different way by considering the energy versus wave vector relation in Figs. 4(a) and 4(b) which show the dispersion of the first and third magneto-electric subbands respectively.

At $B=0$, velocity (slope of the curves) at $k=0.01/\text{Å}$ are nonzero for both the $e1$ and $e3$ subbands. However, the Lorentz force is zero because $B=0$ and hence $d_{e1-e3}=0$. At $B=5$ T, the group velocities for the two subbands are still nonzero and the Lorentz force is finite resulting in skewing of wave functions and a nonvanishing value of d_{e1-e3}. At $B=10$ T, the group velocities at $k=0.01/\text{Å}$ are zero in both subbands indicating that the corresponding states have undergone Landau condensation. In this case, the Lorentz force (for skewing) is again zero and the dipole moment d_{e1-e3} vanishes once more. The crucial point to note is that the Lorentz force $e\vec{v}\times B$ can vanish in two different ways: (i) $B=0$, and (ii) $\vec{v}=0$. These two conditions are met at zero and very high magnetic fields. As a result, the dipole moment d_{e1-e3} exhibits a nonmonotonic behavior in magnetic field. One can ask why the same physics does not cause nonmonotonicity in the $e1$-$e2$ and $e2$-$e3$ curves. It is not clear *a priori* that nonmonotonicity cannot occur (indeed

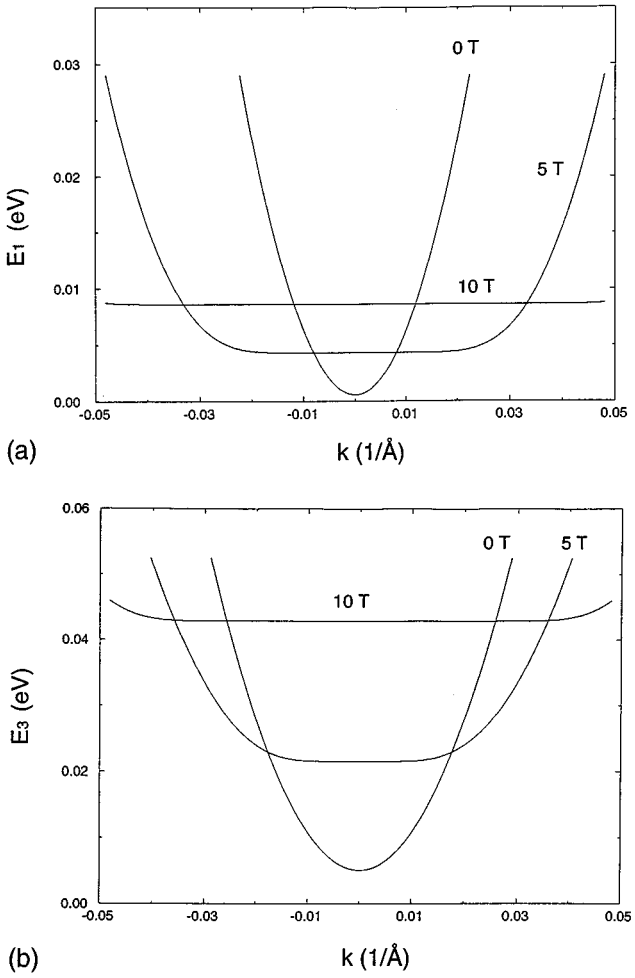

FIG. 4. Energy vs wave vector relation of electrons in (a) the first subband and (b) in the third subband of a 1000 Å wide quantum wire. The wave vector is along the free propagation direction. The results are shown for three values of a magnetic field. The energy is calculated from the bulk conduction band edge and the confinement energy for the z-direction is assumed to be zero.

there are regions of inflexion in the two curves). However, the point to note is that Landau condensation causes recovery of the wave function symmetry (or antisymmetry), *but does not restore the original zero-field wave functions*. This is shown in Fig. 5 where we show the wave functions in the $e1$ subband at 0 and 10 T. Both wave functions are ''symmetric'' in space, but they are otherwise vastly different since the magnetostatic confinement squeezes the wave functions binding them in cyclotron orbits.

The nonmonotonicity in the wave vector dependence of d_{e1-e3} in Fig. 2 has a similar origin. As k is increased, the *relative* skewing between the wave functions in $e1$ and $e3$ subbands change nonmonotonically causing the nonmonotonicity seen.

The process described above is illustrated in Figs. 6(a)–6(c), where we present wave functions of two electronic states ($e1$ and $e3$) for three values of magnetic flux density. At zero magnetic field the wave functions are symmetric about the center of the wire and dipole transition d_{e3-e1} is forbidden [Fig. 6(a)]. At low magnetic field the wave functions are skewed to the edge of the wire [''edge states'' Fig.

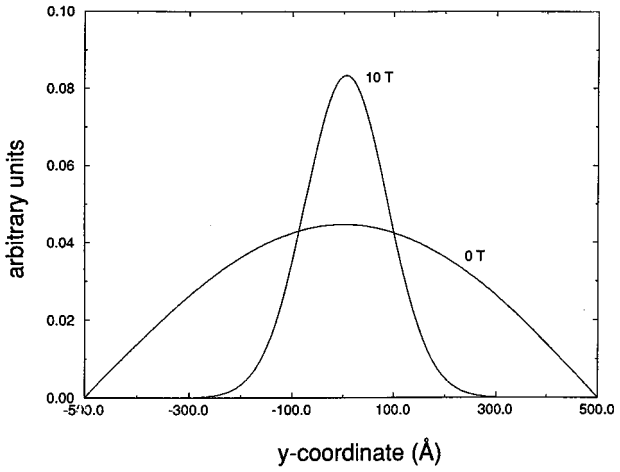

FIG. 5. The y component of the electron envelope function for the first subband at a magnetic flux densities of 0 and 10 T.

6(b)] and the spatial symmetry is broken for both states. Dipole transition d_{e3-e1} is now allowed. It is important to note here that the symmetry breaking skewing of the wave functions is caused by the simultaneous presence of a magnetic field and the electrostatic potential barriers at the edges of the quantum wire. At higher magnetic fields, when the magnetic length is smaller than the wire width, the electrons do not ''feel'' the potential barriers at the edges of the wire as they undergo complete Landau condensation and execute cyclotron motion with a radius much smaller than the width of the wire. In this case, the wave function symmetry is essentially restored [Fig. 6(c)] although the wave functions are now symmetric about a point that is not at the center of the wire. Nonetheless, what is important is that both wave functions are symmetric about the same point. Consequently, the d_{e3-e1} transition vanishes. The simultaneous presence of both electrostatic confinement and magnetostatic confinement is therefore necessary for wave function skewing, formation of edge states and the observation of forbidden transitions.

B. Second-harmonic generation

It is well known that in systems with inversion symmetry there can be no second order nonlinearity.[8] However, in systems without inversion symmetry, the lowest order optical nonlinearity is of the second order and is expressed by

$$\vec{P}^{(2)}(\vec{k},\omega)=\chi^{(2)}(\omega;\omega_1,\omega_2)\vec{E_1}(\vec{k_1},\omega_1)\vec{E_2}(\vec{k_2},\omega_2), \quad (9)$$

where $\vec{P}$ is the polarization caused by two electric fields $\vec{E}_1$ and $\vec{E}_2$ that are associated with the electromagnetic fields of either two frequency components of the same light beam or two different coherent beams with frequencies ω_i and wave vectors $\vec{k_i}$. The frequencies and wave vectors obey the energy and momentum conservation laws

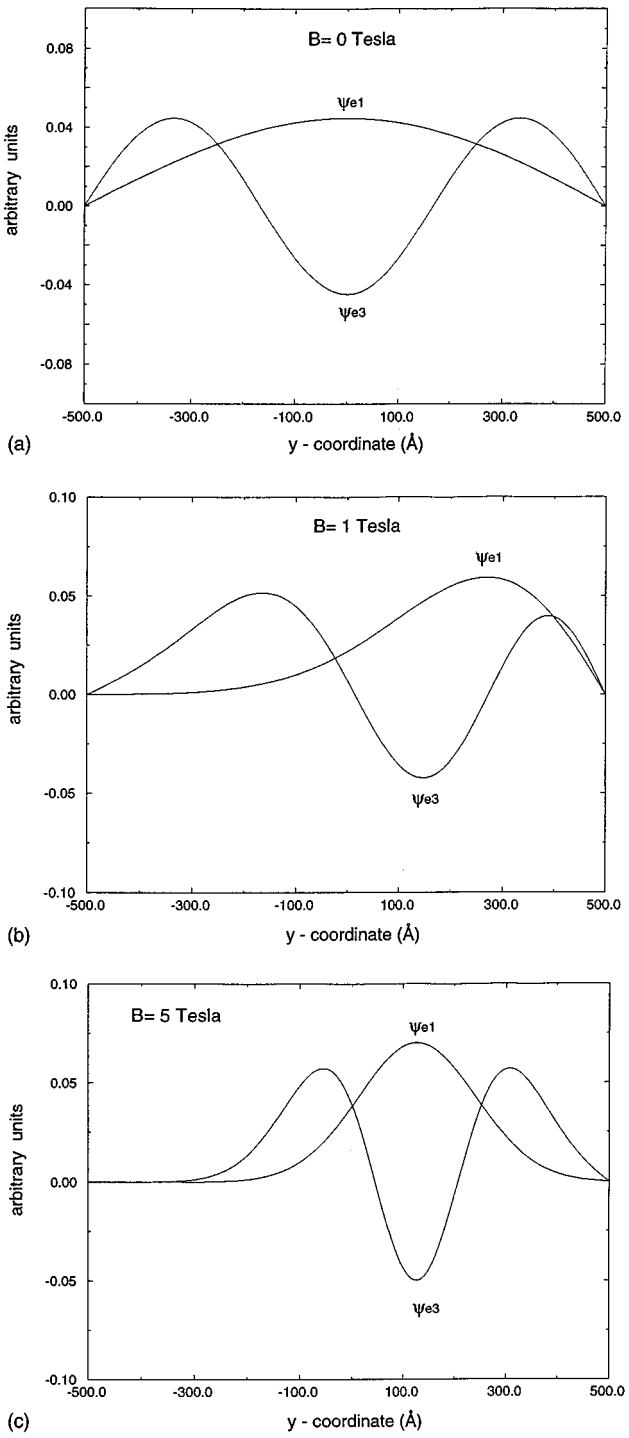

FIG. 6. The y component of the electron envelope functions for the first and third electronic subbands. The results are shown for cases when (a) no magnetic field is present, (b) when a weak magnetic field is present and, finally, (c) when a strong magnetic field is present.

$$\hbar\omega=\sum_i \pm\hbar\omega_i,$$
$$\hbar\vec{k}=\sum_i \pm\hbar\vec{k_i}. \quad (10)$$

It is obvious that the third-ranked tensor $\chi^{(2)}$ will vanish in any structure with inversion symmtery. A quantum con-

fined structure may lack inversion symmetry for two main reasons. (i) The semiconductor material by its intrinsic chemical and crystalline structure may lack inversion symmetry,[9] and this is the case in most III–V, II–VI, and I–VII compounds along certain crystallographic directions. (ii) The quantum confining potential well may be asymmetric (e.g. triangular potential well, asymmetric double square well potential, etc.). In the first case, the asymmetry is related to the intracell charge asymmetry and is not affected by the confinement since the latter extends over several unit cells. In the second case, the asymmetry is artificially imposed and therefore can be engineered. It clearly depends on the confining potential and hence an applied electric field can alter the potential and change the degree of symmetry breaking.

In the present work we restrict ourselves to the second case and do not consider intrinsic second-order nonlinearities of GaAs which are actually quite large (the nonlinear susceptibility of bulk GaAs is $\chi_{14}^{(2)}=3.8\times10^{-10}$ m/V[10]). As mentioned before, we avoid an electric field since it promotes carrier escape and we consider a magnetic field instead. Although a magnetic field does not affect the potential to first order, the simultaneous action of *symmetric* electrostatic potential and an external magnetic field may lead to the *uneven charge distribution* along the width (y axis) of the wire caused by different degrees of skewing of the wave functions. Because of this reason, it is possible to break the inversion symmetry in a symmetric quantum well or wire with a magnetic field alone. This approach is superior to applying a transverse electric field since the latter will tilt the confining potential wells thereby promoting carrier escape from the well by either tunneling or thermionic emission.

The large magnitude of the dipole moments associated with otherwise forbidden transitions between subbands of the same parity and their sensitivity to the biasing magnetic field opens up the possibility of second-harmonic generation (SHG) that can be controlled by the magnetic field. In order to evaluate the magnitude and dependences of SHG on the biasing field and wire geometry, we calculate the second-order susceptibility using the formula[11]

$$\chi_{\mu\alpha\beta}^{(2)}(-\omega_\sigma;\omega_1;\omega_2)=\frac{Ne^3}{\epsilon_0 2\hbar^2}\widehat{S_T}\sum_{abc}\rho_o(a)\times\left[\frac{d_{ab}^{\mu}d_{bc}^{\alpha}d_{ca}^{\beta}}{(\Omega_{ba}-\omega_1-\omega_2)(\Omega_{ca}-\omega_2)}\right], \quad (11)$$

where N is the concentration (number density) of conduction electrons, $\hbar\Omega_{\alpha\beta}\equiv\hbar\Omega_{\alpha\beta}(B,W)$ is the energy spacing between α,β subbands that depends on the applied magnetic field and wire width, $d_{mn}\equiv d_{mn}(B,W)$ is a dipole element calculated using Eq. (4), and ω_σ is defined to be $\omega_\sigma=\omega_1+\omega_2$. The total symmetrization operation $\widehat{S_T}$ indicates that the expression that follows it is to be summed over all six permutations of the pairs $(\mu,-\omega_\sigma)$, (α,ω_1), (β,ω_2). Since $\widehat{S_T}$ involves a summation over all possible permutations, it is clear that $\chi_{\mu\alpha\beta}^{(2)}(-\omega_\sigma;\omega_1;\omega_2)$ is invariant under any of them. For simplicity, the Fermi distribution $\rho_o(a)$ was assumed to be unity.

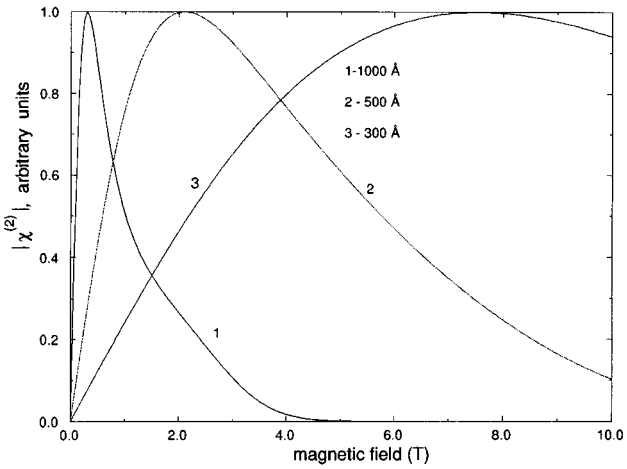

FIG. 7. Second-order susceptibility as a function of the biasing magnetic field. The peak values of the susceptibility are 13.2×10^{-7} m/V, 1.5×10^{-7} m/V and 3×10^{-8} m/V for wire widths of 1000 Å, 500 Å, and 300 Å, respectively. The results are shown for the wave vector $k=0.01$/Å (fixed excitation frequency).

Eq. (11) is an approximation that applies only under the condition that all of the optical frequencies involved (operational frequencies $\omega_\sigma,\omega_1,\omega_2$) are removed far enough from the subband transition frequencies. It means that the medium is assumed to be transparent and loss free at all the relevant optical frequencies. This assumption can be relaxed by the introduction of transition damping factors into the expression in Eq. (11). In our study we are mainly interested in the effects of an applied magnetic field on the second-order susceptibility. Since these effects manifest themselves in Eq. (11) primarily via the magnetic field dependence of the dipole elements $d_{mn}\equiv d_{mn}(B)$, we did not include any damping constants and associated finite linewidths of the electronic states. One should also note here that Eq. (11) is strictly correct only for dilute media. In this case, one can write $\chi^{(2)}=N\alpha^{(2)}$ with $\alpha^{(2)}$ being the second-order nonlinear polarization. The above expression is valid only under moderate excitation.

In Fig. 7, we present normalized values of $\chi^{(2)}$ as a function of magnetic field for three different wire widths and a fixed value of the wave vector k (fixed excitation frequency). The operational frequencies $\omega_1=\omega_2$ are chosen for a CO_2 laser. For wide ranges of magnetic flux densities ($B<20$ T) and wire widths (100 Å $<W<$1000 Å), these frequencies are removed far enough from the subband transition frequencies $\Omega_{\alpha\beta}(B,W)$. As long as the latter is true, the $\chi^{(2)}$ dependence on magnetic field is governed mainly by dipole elements d_{mn}. Consequently, the $\chi^{(2)}$ curve for $W=1000$ Å peaks at the same value of a magnetic flux density ($B=0.3$ T) as the $e1$-$e3$ dipole curve of Fig. 3. The magnetic flux density at which $\chi^{(2)}$ reaches its maximum increases with decreasing wire width. This happens because it takes a higher magnetic field to condense electronic states into cyclotron orbits (Landau condensation) when the electrostatic confinement is stronger (narrower wires).

Fig. 8 shows the dependence of the normalized values of $\chi^{(2)}$ on wire width for three different values of a magnetic

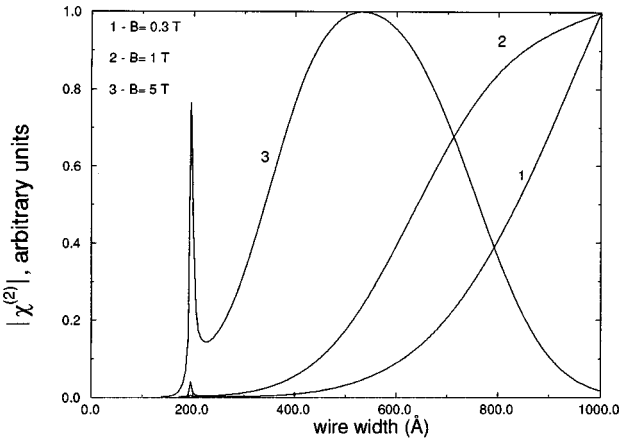

FIG. 8. Second-order susceptibility as a function of the wire width for three values of the biasing magnetic field. The maximum values of the $\chi^{(2)}$ curves are the same as in Fig. 7. The narrow peaks at a wire width of ~200 Å are due to resonances occurring when either $\Omega_{ba}=\omega_1+\omega_2$ or $\Omega_{ca}=\omega_2$.

field and a fixed value of the wave vector. For weak magnetic field of 0.3 T, the $\chi^{(2)}$ curve increases monotonically with increasing wire width. This happens because $d_{m,n}$ is proportional to the wire width W (see Eq. (5) which is valid at zero field). The magnetic field is obviously not strong enough for the onset of Landau condensation. At a moderate magnetic flux density of 1 T, we can observe some saturation features, and for a strong magnetic field of 5 T, the curve is nonmonotonic, rolling down to almost zero for the wire width of 1000 Å. The physics underlying the difference in the behaviors of the three curves is essentially the same as that responsible for the features in Fig. 7. At small values of wire width ($W\approx 170$ Å), there is an additional peak in the $\chi^{(2)}$ curve. This peak is a manifestation of the fact that Ω_{ba} has become comparable to the operational frequencies, i.e. $\Omega_{ba}\approx\omega_1+\omega_2$.

In our numerical calculations we have used $N=10^{17}$ cm^{-3}. For this dilute concentration, high density effects such as screening and bandgap renormalization are not important and Eq. (11) is strictly valid. In fact, Ref. 1 demonstrated excellent agreement between theory and experiment without accounting for any high density effect even though the carrier concentration in that study was $N=5\times 10^{17}/\mathrm{cm}^3$. Therefore, we believe that high density effects are not significant in this regime.

The peak value of the second-order susceptibility for a wire width of 500 Å is $\chi^{(2)}=1.5\times 10^{-7}$ m/V (the absolute magnitudes of the peak values for various wire widths are given in the caption of Fig. 7). For comparison, the nonlinear susceptibility of electric field biased GaAs quantum wells ($W=92$ Å), calculated theoretically and measured experimentally in Ref. 1, was $\chi^{(2)}=2.4\times 10^{-8}$ m/V for an electric field of 36 kV/cm. This shows that relatively weak magnetic fields in quantum wires can produce similar magnitudes of $\chi^{(2)}$ as rather strong electric fields in quantum wells. Unfortunately, to our knowledge, there is no theoretical or experimental result available for either electric field biased quantum wires or magnetic field biased quantum wells so a direct comparison is not possible. Nonetheless, it is obvious that magnetic field biased quantum wires provide a very attractive alternative to other means of producing large $\chi^{(2)}$ values. In fact, the largest value of $\chi^{(2)}$ (obtained at a magnetic flux density of 2 T) in a magnetic-field-biased quantum wire is found to be three orders of magnitude higher than what can be achieved in bulk GaAs.

IV. CONCLUSION

We have theoretically studied the giant dipole effect in magnetic-field-biased semiconductor quantum wires. The dipoles are associated with transitions between magneto-electric subbands within the conduction band, some of which are forbidden in the absence of the magnetic field. The resonant frequencies of these transitions can be tuned by the magnetic field which allows the realization of externally tunable intersubband lasers. We have also studied the possibility of second-harmonic generation in a quantum wire biased with a magnetic field and find a strong second-harmonic component of the susceptibility. This may have important applications in nonlinear optics.

ACKNOWLEDGMENT

This work is supported by the U.S. Army Research Office under Contract Nos. DAAH04-95-1-0586 and DAAH04-95-1-0527.

[1] M. M. Fejer, S. J. B. Yoo, R. L. Byer, A. Harwit, and J. S. Harris, Phys. Rev. Lett. **62**, 1041 (1989), and references therein; L. C. West and S. J. Eglash, Appl. Phys. Lett. **46**, 1156 (1985); for an overview of current work on intersubband transitions, see, for example, *Quantum Well Intersubband Transition Physics and Devices*, NATO ASI Series E270, edited by H. C. Liu, B. F. Levine, and S. Y. Anderson (Academic, Dordrecht, 1994).

[2] A. Sa'ar, I. Grave, N. Kuze, and A. Yariv, *Nonlinear Optics: Materials, Phenomena and Devices*, (IEEE, New York, 1990) 113; B. F. Levine, R. J. Malik, J. Walker, K. K. Choi, C. G. Bethea, D. A. Kleinman, and J. M. Vandenberg, Appl. Phys. Lett. **50**, 273 (1987).

[3] See, for example, Manfred Helm, Semicond. Sci. Technol. **10**, 557 (1995).

[4] E. J. Austin and M. Jaros, Phys. Rev. B **31**, 5569 (1985).

[5] A. Balandin and S. Bandyopadhyay, J. Appl. Phys. **77**, 5924 (1995); A. Balandin, Ph.D. dissertation, University of Notre Dame, 1996.

[6] C. Weisbuch and B. Vinter, *Quantum Semiconductor Structures: Fundamentals and Applications* (Academic, Boston, 1991).

[7] S. Chaudhuri and S. Bandyopadhyay, J. Appl. Phys. **71**, 3027 (1992).

[8] See, for example, J. M. Hvam in *Nonlinear Spectroscopy of Solids: Advances and Applications*, edited by B. Di Bartolo and B. Bowlby (Plenum, New York, 1994), pp. 91–149.

[9] This lack of symmetry is due to the transfer of a valency charge from one atom to the other bond-forming atom and resultant uneven charge distribution along the bond axis.

[10] *Handbook of Lasers*, edited by R. J. Pressley (Chemical Rubber, Cleveland, 1971), p. 504.

[11] See, for example, P.N. Butcher and D. Cotter, *The Elements of Nonlinear Optics* (Cambridge University Press, Cambridge, 1990); A. Yariv, *Quantum Electronics* (Wiley, New York, 1989); or Y. R. Shen, *The Principles of Nonlinear Optics* (Wiley, New York, 1984).